3-D ultrasonic medical imaging based on segmented annular arrays.

Luis G. Ullate*, Oscar Martínez*, Gregorio Godoy†, Alberto Ibáñez*

**Instituto de Automática Industrial (CSIC), La Poveda, Arganda del Rey, 28500, Madrid*
e-mail: luisg@iai.csic.es
†*Departamento de Electrónica, Universidad de Jaén*, e-mail: ggodoy@ujaen.es

Abstract

Conventional 2D ultrasonic arrays are formed by square elements, which have a limit of λ/2 spacing. In this paper we present two apertures, which are based on segmented annular (SA) arrays that have the property of producing lower grating lobes and, consequently, that allow increasing the size of the elements. With the purpose of designing apertures of medium size (D=30λ) with a reduced number of active elements (<250), several thinned squared and segmented-annular arrays are here analyzed. A thinning technique valid for SA arrays that is a modified version of the vernier sparse method ("single vernier") is presented. The paper shows that SA arrays may produce images with similar properties than squared arrays, but with a signal intensity around 20 dB above.

1 Introduction

Two-dimensional (2-D) ultrasonic arrays are useful for volumetric imaging in medicine, because they produce steered and focused beams throughout a volume of interest. Typical 2-D arrays are based on a squared matrix configuration, where the array elements are the cells of the matrix [1]. Due to the aperture periodicity, the inter-element spacing is maintained near λ/2 in order to avoid grating lobes [2]. This condition gives rise to several problems: first, the number of array elements becomes too high in relation to the number of channels of the existing ultrasonic imaging systems. A second problem derives from the small size of the elements that causes a great increase in the electrical impedance and, consequently, a reduction in the signal to noise ratio [1].

Recently, thinning techniques have been proposed to reduce the number of active elements without producing a notable deterioration of the image. One approach eliminates periodicity, and therefore grating lobes, by randomly selecting a subset of elements from the array transducer [2]. As a consequence of random sparse, sidelobes form a "pedestal" surrounding the main beam, whose level is inversely proportional to the number of active elements. A different approach uses two complementary arrangements for transmitting and receiving (T-R) as a way of suppressing grating lobes. Concretely, in Reference [3] using a vernier scale the elements can be separated by distances of multiple of λ/2. In both methods, the number of active elements can be reduced by one order of magnitude with good results on the beam-forming properties of the array. However, the dramatic reduction of the ultrasonic energy due to the extremely low emitting area of sparse arrays is still a great drawback of the imaging system. For instance, the transmission-reception transducer area of a 30λ-diameter aperture is $714\lambda^2$, and it is reduced to $64\lambda^2$ for a 256-channel imaging system of λ/2 inter-element spacing.

In this work, we present a different approach for 3D medical imaging that is based on 2-D segmented annular (SA) arrays. Circular arrays have lower periodicity and, consequently, lower grating lobes than squared arrays. This characteristic allows SA array transducers to have inter-element spacing larger than λ/2 and, at the same time, to increase the size of elements in relation to squared arrays [4].

Our goal is to design apertures with a reduced number of active elements that can be controlled by an imaging system with up to 256 channels. In the following sections we make a theoretical comparison of the image properties of squared and segmented annular arrays of medium size (D=30λ). All simulations are based on the following example: an array with D=15mm emitting waves into water with 3MHz of central frequency and 50% of relative bandwidth. Comparisons are made in pulse-echo for a target point deviated 30º in elevation from the array axis and considering a fixed focus in transmission and dynamic focusing in reception.

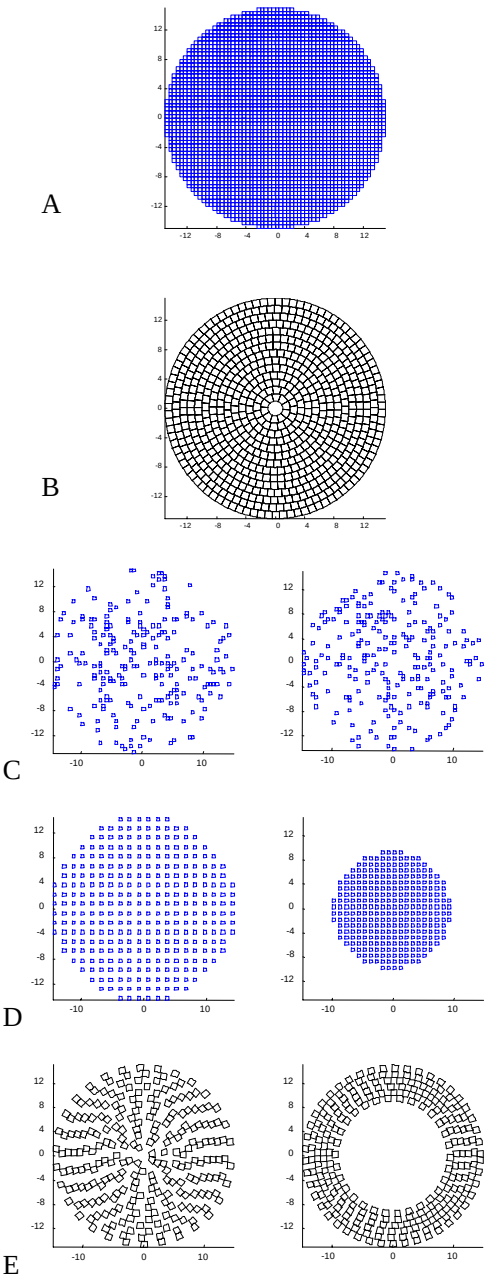

Figure 1. Arrays studied in this paper (dimensions are given in units of λ): (a) squared pattern array with λ/2 interspacing, (b) segmented annular array (SAA) with λ interspacing, (C) random sparse R-T arrays (C), vernier sparse R-T arrays (D), R-T vernier sparse from SAA

2 Array configurations

Five aperture configurations have been considered in our comparisons. The first one (C1) is a full array formed by 0.5λ*0.5λ square elements spaced at a distance of λ/2 (figure 1-a) within a 30λ diameter aperture. This array has 2828 elements that are active in transmission and in reception and the active area is $707\lambda^2$. Although the array does not fulfill the designing conditions due to the excessive number of elements, its beam characteristics are considered a "gold standard" for comparisons with the rest of apertures.

The second aperture (C2) is a ring divided array whose elements are formed by annular segments with λ*λ of medium size, which are spaced λ (figure 1-b). The full aperture contains 707 elements, which are active in transmission and in reception. This configuration also fails to fulfill the designing conditions, but it is analyzed to show the capability of annular arrays in relation to dense squared arrays, after dividing by four the number of elements.

Configurations C3 and C4 are sparse designs from C1 for the purpose of reducing the number of active elements. C3 is formed by randomly selecting 230 active elements from C1 (sampling factor = 1/12). In order to increase diversity, two different random distributions have been used for transmission and reception (Figure 1-c). C4 has been formed from C1 by applying a third-order vernier sparse technique [3]. In this case (Figure 1-d), the receipt aperture is formed by sampling C1 with a pitch of 3 in the two main directions of the array and the transmission aperture is formed in a similar way but with a pitch of 2. In this way, two complementary apertures are obtained with 308 elements each (the reducing factor is 1/9) and $77\lambda^2$ of active area.

The fifth configuration has been created from C2, applying a modified version of the vernier technique (figure 1-e) in the following way: in the tangential direction, we apply a third-order vernier reduction, selecting in all rings one active element every three elements in reception and every two elements in transmission; however, we do not apply any reduction in the radial direction. By this way, the number of active elements of the full aperture is divided by 3, becoming an aperture of 230 elements and $230\lambda^2$ of active area.

3 Computational method

For simulations we assume a 2-D array lying in the Z=0 plane of a Cartesian coordinate system. We consider that the elements ideally vibrate like pistons with a velocity v(t). The array emits sound waves, which propagate with a velocity c through a homogeneous liquid medium of density ρ. We consider an infinitely rigid baffle for boundary conditions and, therefore, a constant obliquity factor β=2. The pressure waveform p(.) radiated over a field point $\bar{x}$ (r,ϕ,θ) (given in spherical coordinates) is:

$$p(\bar{x},t)=\frac{\rho}{c}\frac{dv(t)}{dt}*\sum_{i=1}^{N}h_i(\bar{x},t-T_i)=\frac{\rho}{c}\frac{dv(t)}{dt}h_A(\bar{x},t) \quad (1)$$

Where $h_i(.)$ is the spatial impulse response function of the i^{th} array element located at $\bar{x}_i$ (r_i,ϕ_i,π/2), (*) indicates temporal convolution, $h_A(.)$ is the array impulse response and T_i are time delays for focusing the beam at the point $\bar{x}^F$ (r^F,ϕ^F,θ^F) :

$$cT_i=\left|\bar{x}^F-\bar{x}_i\right|-\left|\bar{x}^F\right| \quad (2)$$

The transmit-receive mode case has been simulated considering that the received signal *s(t)* due to a reflecting point in $\bar{x}$ is given by:

$$s(\bar{x},t)=\frac{\rho^2}{c^2}\frac{dv^2(t)}{dt^2}\left\{h_A{}^T(\bar{x},t)*h_A{}^R(\bar{x},t)\right\} \quad (3)$$

where $h_A{}^T$ and $h_A{}^R$ are the transmit and receive impulse response functions of the array. In general, these functions are not coincident, because both the aperture and delay functions for transmitting and receiving are different.

There are several works which describe methods to calculate the impulse response function of a squared transducer [5] or a segment of annulus [6]. In this case, we will directly compute the Railley integral according to the method indicated in ref. [7]. Dividing the elements into square cells of side s (s≤λ/8), the impulse response corresponding to the i^{th} element can be calculated by:

$$h_i(\bar{x},t)=s^2\sum_{k=1}^{N}\delta(t-\left|\bar{x}-\bar{x}_k\right|/c-T_i) \quad (4)$$

where k=1…N refers to the square cells within the i^{th} array element.

4 Simulation results

Our simulations have been made in pulse-echo for a target point deviated 30º in elevation from the array axis and considering fixed focus in transmission at a distance that is half of the far-field (r^F=60mm) and dynamic focusing in reception. We assume that the transducer size is D=15mm, and that itemits into water (c=1500m/s) a gaussian pulse of 3MHz central frequency (λ=0.5mm) and of 1.5MHz bandwidth at –6dB. Two different 2-D images are analyzed: Figure 2 shows beam plots, which have been obtained at the focal distance (r=60mm), scanning the array in the elevation direction (-60º≤θ≤60º) and in the azimuth direction (0º ≤ϕ≤ 180º). Figure 3 shows B-class images of the $\phi = 0º$ plane, which have been obtained scanning the beam in elevation (–90º≤θ ≤+90º), for target points at several depths in the range of 20mm≤r≤120mm. These two-dimensional plots have been drawn for the following contour levels: -20dB, -30dB, -40dB and -50dB.

4.1 Full array transducers

Figure 1(a) shows a squared pattern dense array, with 2828 elements (C1). Figure 2(a) shows the image of a target point, which is deviated 30º from the array axis, and which has been obtained in the conditions above cited. This can be taken as a gold standard in relation to other array configurations.

Table 1 shows the computed width of the main beam for different amplitude levels. The width at –6dB approximates to the theoretical value given in [8]:

$$\alpha=0.94*asin(\frac{\lambda}{D\cdot\cos\theta}) \quad (5)$$

Due to the side lobes, the width at –40dB is 8.8º, which is relatively high. An explanation for this lies in the non-regular perimeter of the aperture. The main advantage of using λ/2 interelement spacing is that grating lobes are very low. In figure 2(a) we can observe that grating lobes are concentrated in the main directions of the array starting from θ=-40º and growing to –60dB.

	C1	C2	C3	C4	C5
α (-6dB)	2.2º	2.4º	2.3º	2.5º	2.2º
α (-20dB)	4.2º	4.4º	4.4º	4.5º	3.8º
α (-40dB)	8.8º	8.3º	6.7º	7.5º	11º

Table 1: Angular width of the main beam at different levels (in dB).

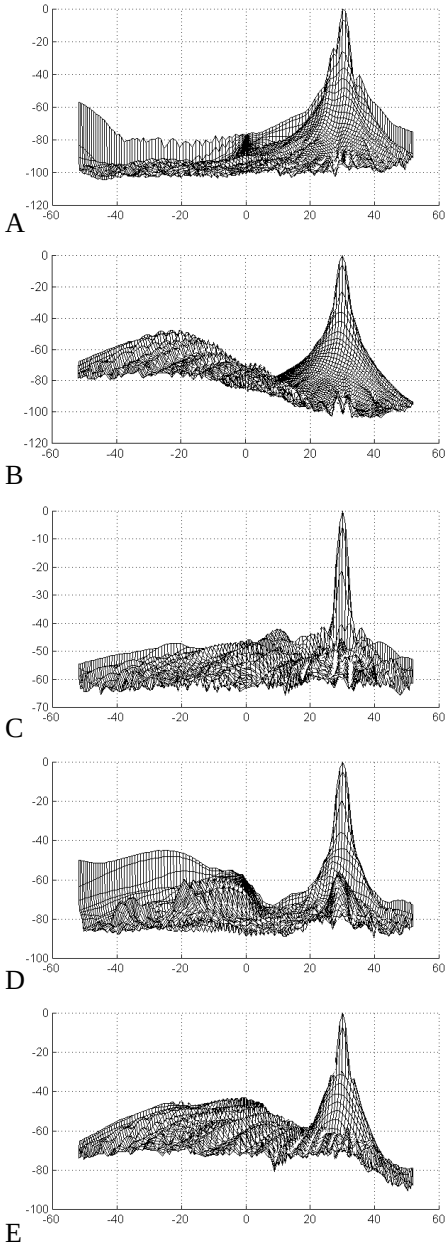

Figure 2. Beam profiles for a target point at (r=60mm, θ=30º, ϕ=0º) for the five array configurations: C1 (a), C2 (b), C3 (c), C4 (d), C5 (e). Vertical axis: amplitude in dB, Horizontal axis: θ

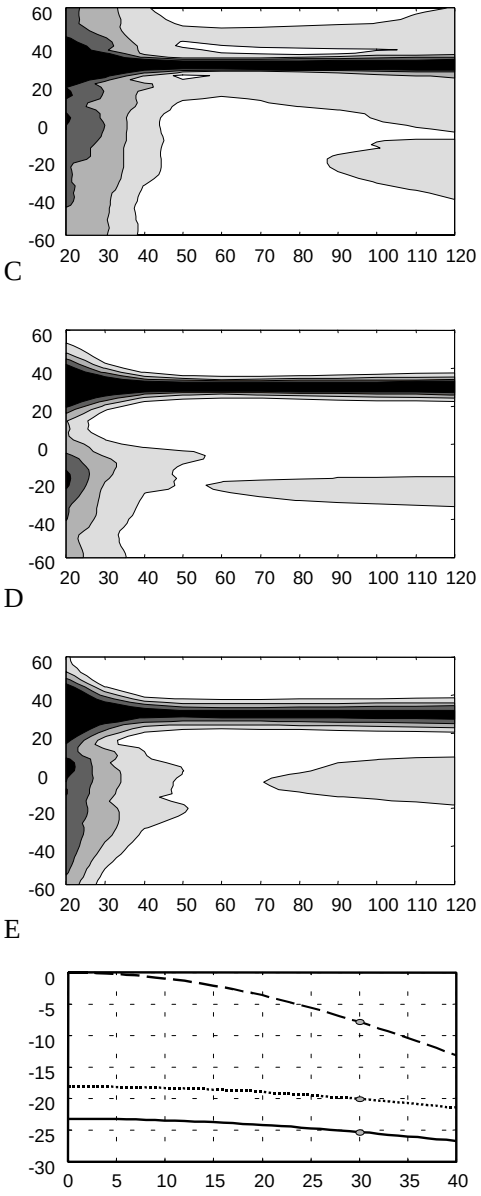

Figure 3. Relative B-class images (normalized in depth) for target points at (20≤r≤120mm θ=30º, ϕ=0º) for the sparse arrays: C3 (c), C4 (d), C5 (e). (Axis: r(mm),θ(º). Contour levels: -20dB, -30dB, -40dB, -50dB). <u>Lower part</u>: Lateral response in amplitude : C3 (-), C4 (..), C5(--). Axis: [θ(º), peak of amplitude (dB)]

This is a very reasonable contrast level for medical imaging, where a contrast of –50dB is typically demanded [2], but this solution requires controlling an excessive number of array elements. In order to reduce the number of elements without loosing active area, the element size must be increased. However, an increase in grating lobes will excessively reduce the image contrast (i.e.: using a squared array D=30λ with 707 elements λ∗λ, grating lobes will increase to –19dB).

Figure 1(b) shows a ring divided array (C2) with 707 elements of size λ∗λ. The beamplot characteristics can be observed in figure 2(b) and the main beam width is given in Table 1. From the table values, we can deduce a slight deterioration in the upper part of the beam, which is mainly due to the greater size of the elements. However, the regular perimeter of the array makes the main lobe at –40dB to be narrower than in the C1 case. On the other hand, ring divided arrays produce grating lobes, which spread over a large area, but their amplitude is reduced. In Figure 2(b), the grating lobe level of C2 is –48dB, which can still be allowed for ultrasonic imaging.

4.2 Sparse array transducers

The number of elements can be reduced by selecting a fraction of the elements in reception and in transmission. There are several ways of designing sparse apertures without greatly increasing grating lobes. Figure 1(c-d) shows two types of sparse arrays typically proposed in literature, which have been derived from the squared aperture C1. The random sparse array has 230 elements, which is reasonably near 256, the maximum number of channels of the imaging systems. A third-order vernier array is used, implying 308 elements in the aperture (>256). In contrast to random arrays where we can select the number of elements at will, the reduction of a vernier array of n^{th} order is N/n^2 (N: elements of the full array), which supposes a serious limitation in the choice of the number of elements. In our case, a fourth order vernier will give an aperture with only 176 elements, far from 256.

Figure 1(e) shows a sparse aperture designed from the annular array C2. The thinning function is a modified version of the vernier method (we call the single-vernier method), because the selection is only in the tangential direction but not in the radial one. In this way, the sparse reduction is N/n, which that allows a better design than the above mentioned typical verniers. In this case, we have chosen a third-order single-vernier, resulting in 230 elements in the aperture. In this case, the aperture with pitch=2 occupies a fraction of the array area, typically reducing the aperture diameter. In our case, we present another solution by selecting the outer part of the array.

From Figure 2, the image properties at the transmission-reception focal plane can be analyzed. From Table 1 it is deduced that the main beam of C5 is narrower up to –34dB, mainly due to the ring effect. From that level, side lobes widen the beam more than the other solutions. On the other hand, the main beam width of random sparse arrays is narrower than the vernier ones, for two reasons. First they do not have the first side lobe, which is caused by the array border, and second, the vernier array has lower resolution due to the small size of the transmission aperture. Looking at the secondary lobes, we can observe that apertures C3 to C5 give results very similar in amplitude around –45dB, although the vernier solution has the grating lobes at elevation angles farther from the steering direction. This is an advantage if we consider soft baffle in the boundary conditions, as these amplitudes would be affected by a factor of approximately cos(θ). However, it should be noted is that C5 is formed by λ*λ elements, while C3 and C4 are λ/2*λ/2.

Figure 3 (c-d) shows the beam behavior for a large depth, from $D^2/24\lambda$ (20mm) to the farfield distance (120mm). The level contours correspond to –20dB, -30dB, -40dB and –50dB. With respect to the main lobe, we can observe that C5 has a narrower main beam for levels upper –30dB for practically all distances from 40mm. In this sense, the random sparse array also has very good behavior for levels higher than –40dB. On the other hand, for all distances from 35mm, the three apertures present B-class images with a secondary lobe level under –40 dB. In this sense, the random sparse array C3 has a greater density of secondary lobes, while the vernier C4 shows the lower density.

If we consider only normalized parameters, from Figures 2 and 3 it is deduced that the sparse arrays analyzed here present an almost similar capability for generating ultrasonic images. However, a great advantage of C5 can be observed in the lower part of Figure 3, where the peak of amplitude of the received signals is represented as a function of the elevation θ^F of the target point. Comparing the curves from C3 and C5 (they have the same number of elements), it is observed that C5 produce signals 24 dB above C3 for the normal direction (θ=0º) and 17 dB above for θ=30º. The larger drop of the C5 curve is due to the narrower radiation pattern of elements in C5. The C4 array produces a curve very similar to C3 but it is 5dB

above because of its greater number of elements $20\log(N_{C4}/N_{C3})^2$.

5 Conclusions

We have analyzed the capability of segmented annular (SA) arrays for ultrasonic imaging in medicine. In this sense, we have shown that SA arrays allow designing 2-D array transducers with inter-element spacing larger than λ/2. We have made theoretical simulations for 5 array configurations of medium size (D=30λ). Two SA array configurations whose elements have a size of λ*λ have been analyzed: (a) the full array with 707 elements and (b) a third-order "single vernier" array with 230 elements. From simulations we deduce the following conclusions for medium apertures: (1) SA array transducers allow applying vernier techniques only in one direction ("single vernier") and, consequently, the reduction is proportional to the vernier order. This facility is useful for adjusting better the number of active elements to the image system capability; (2) a sparse SA array transducer produces images of similar quality to that of typical sparse squared arrays, but it may produce signals which are 20 dB of higher intensity. (3) As SA array transducers allow designs with elements several times larger than typical squared arrays (four times in the examples of this work), the problem of electrical impedance and, consequently, of the signal to noise ratio typical of squared arrays is reduced.

Acknowledgement

This work received the assistance of CICYT (Spain), FEDER-2F97-1581 and FEDER-2F97-2290 projects.

References

[1] Light, E.D., Davidsen, R.E., Fiering, J.O., Hruschka, T.A., "Progress in Two-Dimensional Arrays for Real-Time Volumetric Imaging", *Ultrasonic Imaging*, 20:1-15, 1998

[2] Turnbull, D.H., Foster, F.S., "Beam Steering with Pulsed Two-Dimensional Transducer Array", *IEEE Trans. on Ultrasonics, Ferroelectrics and Frequency Control*, 38:320-333, 1991

[3] Brunke, S., Lockwood, G, "Broad-Bandwidth Radiation Patterns of Sparse Two-Dimensional Vernier Arrays" *IEEE Transactions on Ultrasonics, Ferroelectrics and Frequency Control*, 44:1101-1109, 1997

[4] O. Martínez L.G. Ullate, A. Ibañez "Comparison of CW beam patterns from segmented annular arrays and squared arrays". *Sensors and Actuators* 85, pp.33-37. 2000

[5] J.L.San Emeterio, L.G.Ullate**,** "Diffraction impulse response of rectangular transducers", *J. Acoust. Soc. Am*., vol. 92, no. 2, 1992, pp. 651-662

[6] Oscar Martinez, Francisco Montero, Luis G. Ullate, "Computation of the ultrasonic field radiated by segmented-annular arrays", Journal of Computational Acoustics, (accepted)

[7] Piwakowski, B., Khalid, S., "A New Approach to Calculate the Field Radiated from Arbitrarily Structured Transducer Arrays" IEEE Transactions on Ultrasonics, Ferroelectrics and Frequency Control, 46:422-440, 1999

[8] O. Martínez, "Arrays de anillos segmentados para la generación de imagen ultrasónica 3D", Ph. D. Dissertation, U.P.M., 2000